

Efficiently Training Time-to-First-Spike Spiking Neural Networks from Scratch

Kaiwei Che^{1,2} Wei Fang^{1*}, Zhengyu Ma², Yifan Huang^{2,3}, Peng Xue^{2,4}, Li Yuan¹,
Timothée Masquelier⁵, Yonghong Tian^{1,2,3*}

¹ School of Electronic and Computer Engineering, Shenzhen Graduate School, Peking University, China

² Peng Cheng Laboratory, China, ³ School of Computer Science, Peking University, China

⁴ Shenzhen Institute of Advanced Technology, Chinese Academy of Sciences

⁵ Centre de Recherche Cerveau et Cognition (CERCO), UMR5549 CNRS - Univ. Toulouse 3, France

Abstract

Spiking Neural Networks (SNNs), with their event-driven and biologically inspired operation, are well-suited for energy-efficient neuromorphic hardware. Neural coding, critical to SNNs, determines how information is represented via spikes. Time-to-First-Spike (TTFS) coding, which uses a single spike per neuron, offers extreme sparsity and energy efficiency but suffers from unstable training and low accuracy due to its sparse firing. To address these challenges, we propose a training framework incorporating parameter initialization, training normalization, temporal output decoding, and pooling layer re-evaluation. The proposed parameter initialization and training normalization mitigate signal diminishing and gradient vanishing to stabilize training. The output decoding method aggregates temporal spikes to encourage earlier firing, thereby reducing the latency. The re-evaluation of the pooling layer indicates that average-pooling keeps the single-spike characteristic and that max-pooling should be avoided. Experiments show the framework stabilizes and accelerates training, reduces latency, and achieves state-of-the-art accuracy for TTFS SNNs on MNIST (99.48%), Fashion-MNIST (92.90%), CIFAR10 (90.56%), and DVS Gesture (95.83%).

1. Introduction

Spiking Neural Networks (SNNs), the third-generation neural models [1], mimic biological systems through event-driven spike communication. This paradigm enables energy-efficient computation (up to 100× improvements) validated by neuromorphic hardware like TrueNorth [2], Loihi [3], and Tianjic [4]. Biological plausibility of SNNs makes them valuable tools for neuroscience research [5, 6]. While synaptic plasticity methods like Hebbian learning [7] and Spike-Timing-Dependent Plasticity (STDP) [8] en-

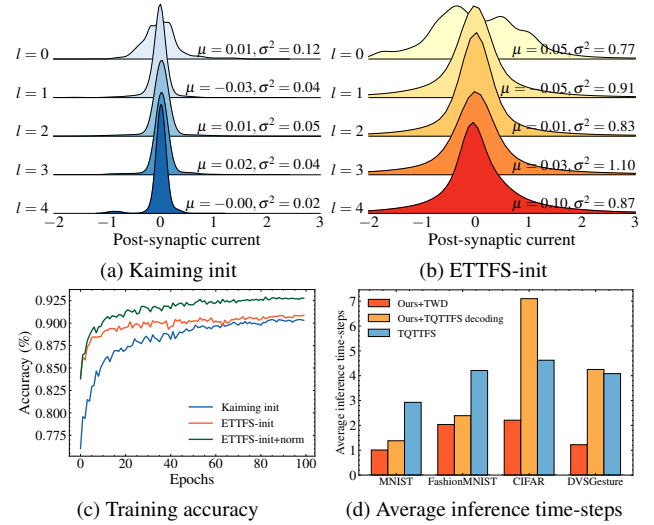


Figure 1. An overview of the impacts and performance of the proposed methods. (a) The default Kaiming initialization causes the signal diminishing problem in the TTFS SNNs, where post-synaptic current variance (σ^2) rapidly decreases across layers (L). (b) Proposed ETTFs-init regulates distributions. (c) ETTFs-init accelerates convergence and improves accuracy over Kaiming initialization, further enhanced by weight normalization. (d) Our decoding method reduces average inference time-steps compared to previous TQ-TTFS decoding [35] across four datasets.

able bio-inspired SNNs training [9–11], they often yield suboptimal performance. Recent advancements integrating powerful deep learning methods to SNNs have significantly boosted performance [12–17], driven by novel spiking neuron models [18–21], network structures [22–29], normalization methods [30, 31], and software frameworks [32–34], etc. Bridging neuroscience and computational science, SNNs gain increasing research attention.

Neural coding, fundamental to SNNs, governs how in-

*Wei Fang and Yonghong Tian are corresponding authors.

formation is represented through spikes. Different biological systems employ diverse mechanisms. Rate coding, where firing rates correlate with stimulus intensity, was first identified in biological systems [36] and proved ineffective for rapid processing. For instance, flies respond to stimuli within 30 ms using just 1-2 spikes [37], necessitating alternative coding mechanisms. Temporal coding methods encode information through precise spike timing. Key biological examples include: Time-To-First-Spike (TTFS) in human visual systems [38], phase coding in rat hippocampus using oscillation phases [39], and rank-order coding in mouse retinal ganglion cells employing spike arrival sequences [40, 41]. Inspired by these biological evidence, neural coding methods for SNNs are proposed. Rate coding dominates ANN-to-SNN conversions [42–46] and direct training sometimes via Poisson encoding [47–50]. Temporal coding adaptations include: TTFS coding mapping ANN activations to spike times [51] or enforcing single-spike constraints [52, 53], burst coding using graded spikes (scalar-spike products) [54, 55], and phase coding employing weighted spike encoding [56, 57].

Among the existing coding methods, TTFS coding communicates by the timing of first spike, which brings rapid information processing ability for humans and animals [38, 58–60]. Its SNN implementation enforces single-spike firing without requiring extra parameters, such as the scalar in burst coding or the temporal weights in phase coding, thereby offering extreme sparsity and energy efficiency for neuromorphic hardware. These distinguished characteristics have attracted increasing interest from the SNN community, and serial research about TTFS SNNs are reported including the ANN-to-SNN conversion methods [51, 61, 62] and the directly training methods [35, 53, 63, 64]. However, the rigorous restriction of spike numbers brings a huge challenge to training TTFS SNNs, and their accuracy is much lower than traditional SNNs. In this article, we address TTFS SNN training challenges through an efficient framework comprising parameter initialization, weight normalization, temporal decoding, and pooling analysis. Our contributions are as follows:

1. We identify the signal diminishing problem caused by Kaiming initialization in TTFS SNNs (Figure 1a) and solve it by proposing a novel parameter initialization method (ETTFS-init), which stabilizes the mean and variance of post-synaptic currents across layers, resulting in a stable distribution (Figure 1b).
2. We apply the normalization method to weights to prevent distribution shift during training, which accelerates convergence and achieves higher accuracy (Figure 1c).
3. We propose a novel temporal weighting decoding to encourage early firing to reduce latency. Figure 1d shows that the proposed decoding dramatically decreases the number of inference time-steps.

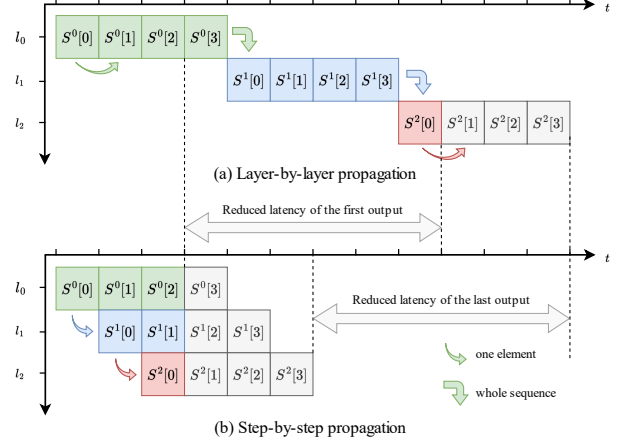


Figure 2. Physical latency comparison in a 3-layer SNN ($T = 4$): Layer-by-layer propagation (common in prior TTFS SNNs) requires each layer to process full input sequences, causing latency scaling with network depth. Step-by-step propagation (our method) enables immediate spike transmission between layers at each time-step.

4. We re-evaluate the pooling layers in TTFS SNNs and recommend using average-pooling to keep the one-spike characteristic, which is the precondition of the parameter initialization and weight normalization methods.
5. Equipped with the proposed efficient training framework, we achieve state-of-the-art (SOTA) accuracy among TTFS SNNs on several benchmark datasets, including MNIST (99.48%), Fashion-MNIST (92.90%), CIFAR10 (90.56%), and DVS Gesture (95.83%).

2. Related Work

2.1. Neural Coding in SNNs

Neural coding in SNNs represents information through spikes. Rate coding measures average spike counts over time, proportional to input strength, enabling ANN-SNN conversion by aligning ReLU activations with the Integrate-and-Fire (IF) neuron rates [56]. However, its accuracy-latency trade-off requires long time windows for precise rate estimation. Temporal coding methods with fewer time-steps have been explored to overcome the ineffectiveness of rate coding. Extended from phase coding, Kim et al. [56] and Wang et al. [65] encode values to spikes and weights in powers of 2, similar to decimal/binary conversion. Burst coding, utilized by Park et al. [54] and Li et al. [55], is implemented through graded spikes and outperforms traditional rate-based ANN-to-SNN conversion methods.

TTFS coding is employed in conversion methods [51, 61, 62] and directly training methods [35, 53, 64, 66], implemented through two propagation paradigms: layer-by-layer and step-by-step propagation (Figure 2). While math-

ematically equivalent, layer-by-layer propagation is computationally efficient on GPUs during training [32]. However, when deploying SNNs to neuromorphic chips, the target devices of SNNs, the physical latency of layer-by-layer propagation is higher and increases with depth. Layer-by-layer propagation must collect the whole input sequences $\{X^l[0], \dots, X^l[T-1]\}$ firstly, where T represents time-steps, l is spiking neuron layer, and then generate output spikes to the next layer. Although achieving high accuracy comparable to ANNs, its latency increases with network depth, which also implies a layer synchronization, while some neuromorphic chips such as the Speck [67] process spikes between computing cores asynchronously. Step-by-step propagation can output spikes $S^l[t]$ immediately after it receives $X^l[t]$ [35, 53]. This propagation gets rid of the latency problem, but its accuracy is poor, and the improvement of which is the aim of this article.

Currently, high-performance SNNs [18, 27, 29] predominantly employ direct input encoding [68], which directly transmits static inputs (e.g., images) across multiple time-steps. While their internal coding strategies remain unclear, analyses reveal that SNN features resemble those of ANNs with limited temporal information [69], suggesting proximity to rate coding. This approach functionally implements rate coding in the first layer through periodic firing [70], further reinforced by rate-based loss functions that implicitly prioritize firing rate optimization.

2.2. Initialization of Networks

In deep neural networks, stable forward and backward information flow is crucial for effective learning [71, 72]. Proper weight initialization is key to maintaining stability throughout multiple layers of propagation. Similar to recurrent neural networks (RNNs), SNNs face challenges related to both depth and the temporal dimension, making them susceptible to vanishing and exploding gradients [24, 73].

While weight initialization in RNNs is well-studied, research on SNN initialization remains limited. Most researchers use the default parameter initialization method, Kaiming initialization [72], provided by PyTorch, and the experience shows that it works well in most cases. Ding et al. [74] first derive the approximate response curve of spiking neurons, based on which the parameters are initialized to overcome the gradient vanishing problem. However, their methods fail to scale to deep SNNs trained on complex datasets. Rossbroich et al. [75] propose an initialization strategy for the Leaky-Integrate-and-Fire (LIF) neuron with exponential current-based synapses, but cannot extend their methods to stateless synapses, which are predominant in deep SNNs. The major challenge for designing parameter initialization algorithms is that the neuronal dynamics involved with the time dimension of spiking neurons are far more complex than non-linear activations in ANNs.

3. Methods

3.1. At-Most-One-Spike Spiking Neuron Model

The At-Most-One-Spike (AMOS) spiking neuron model [35, 53] is extended from the general discrete-time spiking neuron model [21, 32] with the restriction of firing no more than once. The neuronal dynamics of the AMOS spiking neuron are as follows:

$$H[t] = f(H[t-1], X[t]), \quad (1)$$

$$S[t] = (1 - F[t-1]) \cdot \Theta(H[t] - V_{th}), \quad (2)$$

$$F[t] = F[t-1] + S[t], \quad (3)$$

where $H[t]$ is the membrane potential, $X[t]$ is the input current, $S[t]$ is the output spike, and $F[t]$ is the firing mask at the time-step t . f in Eq. (25) is the neuronal charge function specified for different neurons.

The Heaviside function $\Theta(x)$ in Eq. (26) satisfies $\Theta(x) = 1$ if $x \geq 0$ else 0. Spiking is governed by mask $F[t]$ that accumulates via Eq. (27), with initial states $H[-1] = F[-1] = 0$. When $S[i] = 1$ at time-step i , $F[i] = 1$ prevents subsequent firing. Hence, the neuron can only fire no more than one spike and is named the AMOS spiking neuron (see Supplementary Material for neuronal dynamic details). Compared to traditional spiking neurons, the neuronal dynamics of the AMOS neuron omit the reset mechanism, allowing post-spike resting that could enhance energy efficiency in asynchronous neuromorphic chips.

During training, the neuron is forced to fire a spike at the last time-step $t = T - 1$ if it has not fired from $t = 0$ to $t = T - 2$. This setting is also implemented without the if-else statement by updating $S[T-1]$ as:

$$S[T-1] \leftarrow S[T-1] + 1 - F[T-1]. \quad (4)$$

Eq. (4) is used after Eq. (27) at the last time-step. This setting preserves the one-spike characteristic, which is crucial for theoretical analysis and will be frequently referred to in the following subsections. During inference, the AMOS will not be forced to fire at the last time-step, instead, it runs in step-by-step mode, enabling early stopping when a spike occurs in the last layer.

3.2. Initialization for TTFS SNNs

Weight initialization is critical for ensuring adequate activation across layers in TTFS SNNs. Assume an SNN comprising L fully-connected AMOS spiking neuron layers, here the l -th layer can be formulated as:

$$X^l = S^{l-1}W^l, \quad (5)$$

$$S^l = \text{AMOS}(X^l). \quad (6)$$

$S^{l-1} \in \{0, 1\}^{T \times N_l}$ is the input spike from the $(l-1)$ -th layer, where T is the number of time-steps and N_l is the

number of input features of the l -th layer. $W^l \in \mathbb{R}^{N_l \times M_l}$ is the weight of fully-connected synapses, where M_l is the number of output features. $X^l \in \mathbb{R}^{T \times M_l}$ is the input current for the AMOS spiking neurons. $S^l \in \{0, 1\}^{T \times M_l}$ is the output spike of the l -th layer, and AMOS represents the AMOS spiking neurons.

It is worth noting that S^{l-1} keeps the one-spike characteristic during training. For any $j \in \{0, 1, \dots, N^l - 1\}$, the following equation holds true:

$$\sum_{t=0}^{T-1} S^{l-1}[t][j] = 1. \quad (7)$$

For $X^l[t][i]$, the i -th element of the input current at the time-step t , it is calculated as:

$$X^l[t][i] = \sum_{j=0}^{n-1} S^{l-1}[t][j] \cdot W^l[j][i], \quad (8)$$

where $W^l[j][i]$ denotes the weight of synapse from j -th neuron in the $(l-1)$ -th layer to the i -th neuron in the l -th layer. Let the l -th weight follow a distribution with mean μ_l and variance σ_l^2 . Note that W^l and S^{l-1} are independent. The expectation $\mathbb{E}(X^l[t][i])$ is calculated as:

$$\mathbb{E}(X^l[t][i]) = \sum_{j=0}^{N_l-1} \mathbb{E}(S^{l-1}[t][j]) \cdot \mathbb{E}(W^l[j][i]) = \mu_l. \quad (9)$$

Here Eq.(32) is referred. As suggested by Xavier et al. [71] and He et al. [72], the zero expectation is preferred, and we set $\mu_l = 0$ to ensure $\mathbb{E}(X^l[t][i]) = 0$. Consequently, the expectation $\mathbb{E}(X^l)$ is also zero:

$$\mathbb{E}(X^l) = \frac{1}{TM_l} \sum_{t=0}^{T-1} \sum_{i=0}^{M_l-1} \mathbb{E}(X^l[t][i]) = 0. \quad (10)$$

The variance $\mathbb{D}(X^l[t][i])$ is calculated by:

$$\begin{aligned} \mathbb{D}(X^l[t][i]) &= \mathbb{D} \left(\sum_{j=0}^{N_l-1} S^{l-1}[t][j] \cdot W^l[j][i] \right) \\ &= N_l \sigma_{W^l}^2 \cdot \mathbb{E}(S^{l-1}[t][j]). \end{aligned} \quad (11)$$

Then the variance $\mathbb{D}(X^l)$ is:

$$\begin{aligned} \mathbb{D}(X^l) &= \mathbb{E}((X^l)^2) - \mathbb{E}^2(X^l) = \mathbb{E}((X^l)^2) \\ &= \frac{1}{TM_l} \sum_{t=0}^{T-1} \sum_{i=0}^{M_l-1} \mathbb{E}((X^l[t][i])^2) \\ &= \frac{N_l \sigma_{W^l}^2}{T}. \end{aligned} \quad (12)$$

See Supplementary Material for derivation details. When using Kaiming initialization [72], the default weight initialization in PyTorch, the weight will be sampled from a uniform distribution $\mathcal{U} \left(-\frac{1}{\sqrt{N_l}}, \frac{1}{\sqrt{N_l}} \right)$. It satisfies the zero mean of weights according to Eq. (10). However, according to Eq. (34), the variance is:

$$\mathbb{D}(X^l) = \frac{N_l}{T} \cdot \frac{1}{3N_l} = \frac{1}{3T}. \quad (13)$$

$\mathbb{D}(X^l)$ decays asymptotically to zero as the number of time-steps T increases. Extremely small weights will cause the silence problem during forward propagation, leading to vanishing gradients as the surrogate function produces near-zero values when membrane potentials are distant from the threshold. To maintain initialized weights within a stable range decoupled from T , we set $\mathbb{D}(X^l) = 1$. From Eq. (34), $\sigma_{W^l}^2$ must satisfy $\sigma_{W^l}^2 = \frac{T}{N_l}$. We thus propose ETTFS-init: for layer l (N_l input features) in a TTFS SNN (T time-steps), initialize W^l from the following uniform distribution:

$$W^l \sim \mathcal{U} \left(-\sqrt{\frac{3T}{N_l}}, \sqrt{\frac{3T}{N_l}} \right). \quad (14)$$

For fully-connected layers, N_l denotes the number of input features; for convolutional layers, $N_l = C_{in}^l \cdot N_{kernel}^l$ (input channels \times kernel element). With Eq. (14), the input current for the l -th AMOS spiking neuron layer is stabilized:

$$\mathbb{E}(X^l) = 0, \mathbb{D}(X^l) = 1. \quad (15)$$

3.3. Weight Normalization

Although the ETTFS-init method offers a reasonable starting point, the distribution of weights may shift during gradient descent and consequently violate Eq. (15) during the training process. To address this, we employ weight normalization [76–78] to maintain consistent the distribution of weights:

$$W^l \leftarrow \frac{W^l - \mathbb{E}(W^l)}{\sqrt{\mathbb{D}(W^l) + \epsilon}} \cdot \sigma_{W^l}, \quad (16)$$

where W^l is the weight of the l -th layer, $\mathbb{E}(W^l)$ and $\sqrt{\mathbb{D}(W^l)}$ denote the mean and variance of W^l , respectively; ϵ is a small constant for numerical stability; and σ_{W^l} is the standard deviation of the initial weights determined by Eq. (14) when using ETTFS-init.

Eq. (16) also constrains weight scaling, potentially limiting representational capacity. Inspired by batch normalization [79] and layer normalization [80], which incorporate an additional affine transform to solve the fixed-scale problem, we apply a learnable affine transform to the synaptic output X^l with weight γ^l and bias β^l :

$$X^l \leftarrow \gamma^l X^l + \beta^l, \quad (17)$$

where γ^l is initialized as an all-ones tensor and β^l is initialized as an all-zeros tensor. Note that both the weight normalization in Eq. (16) and the learnable affine transform in Eq. (17) are applied only during training. The affine transform can be absorbed into synapses for inference without normalization. The fused weight \tilde{W}^l and bias \tilde{B}^l of the l -th layer are as follows:

$$\tilde{W}^l = \gamma^l \cdot W^l, \tilde{B}^l = \beta^l. \quad (18)$$

This fusion eliminates computational overhead in inference.

3.4. Temporal Weighting Decoding

Traditional SNN decoding uses output layer firing rates [18, 81], which fails for TTFS networks due to uniform firing rates ($1/T$) across neurons during training.

TTFS coding's temporal nature suggests decoding through earliest spike timing. More specifically, suppose the SNN is designed for a classification task with C classes, and the number of time-steps is T , then the output of the SNN is the tensor $O \in \{0, 1\}^{T \times C}$. The predicted class is:

$$Y_{\text{predict}} = \text{argmin}_i \{t \mid O[t][i] = 1\}. \quad (19)$$

Eq. (19) is used in inference, rather than training. The argmin function is not differentiable, preventing the gradient from being backpropagated through it. Therefore, an effective decoding approach for TTFS SNNs should have two key features: differentiability and emphasis on early firing.

The existing TQ-TTFS method [35] compares membrane potentials but introduce complexity without explicit temporal emphasis. To solve these issues, we propose the temporal weighting decoding method, which aggregates the outputs by decayed temporal weights over time-steps. We only employ the basic math operations to maintain differentiability. To emphasize early firing, we introduce the decoding weight $w \in \mathbb{R}^T$ which decays with time-steps. The decoded output $Y \in \mathbb{R}^C$ is defined as the weighted sum of outputs over time-steps:

$$Y = \sum_{t=0}^{T-1} w[t] \cdot O[t]. \quad (20)$$

We set $w[0] = 1$ and $w[t] > w[t+1]$ for any $t \in \{0, 1, \dots, T-2\}$. The weighting factor w can be set as an exponential decay function:

$$w[t] = \gamma^{-t}, \quad (21)$$

where $\gamma > 1$ is the scaling factor. Figure 3 illustrates an example of temporal weighting decoding with exponential decay weights. A linear decay function can also be considered, which is defined as:

$$w[t] = \gamma \cdot \frac{T-t}{T}. \quad (22)$$

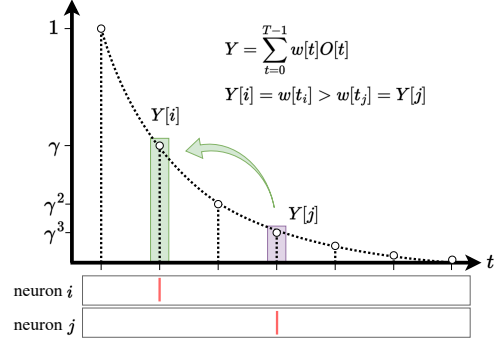


Figure 3. The mechanism of temporal weighting decoding. The weight $w[t]$ is set as an exponential or linear decay function of t . The earlier spike will be decoded to a larger value and predominate the output results. For example, neuron i fires at t_i , which is earlier than neuron j firing at t_j , and $Y[i] = w[t_i] > Y[j] = w[t_j]$.

Eq. (20) is differentiable. At the same time, early firing is privileged. Suppose the i -th AMOS neuron at the output layer fires at time t_i and the j -th AMOS neuron fires at time-step t_j with $t_i < t_j$. It can be found that:

$$Y[i] = w[t_i] > w[t_j] = Y[j]. \quad (23)$$

Derived from Eq. (23), the neuron that has the earliest firing time-step also enjoys the largest decoded value:

$$\text{argmin}_i \{t \mid O[t][i] = 1\} = \text{argmax}_i \{Y[i]\}. \quad (24)$$

3.5. Pooling for One-Spike Characteristic

Pooling layers reduce feature map size and extract compact representations. Prior work [35, 82] uncritically employs max-pooling, but we argue that using average-pooling instead better aligns with the one-spike characteristics of TTFS SNNs. Figure 4 shows a typical example of pooling four AMOS neurons. Max-pooling selects the maximum value within the spatial dimension, potentially violating the one-spike constraint in the temporal domain, while average-pooling keeps the one-spike characteristic perfectly, which is critical for the proposed initialization and decoding methods (See Supplementary Material for precise mathematical description). Notably, average-pooling layer can be merged into the subsequent layer to avoid floating-point computation.

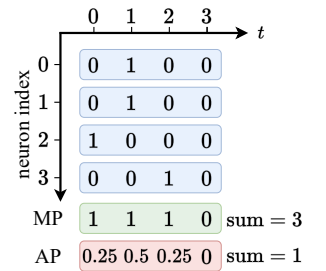


Figure 4. Example of pooling in TTFS SNNs.

Table 1. Comparison on MNIST, Fashion-MNIST, CIFAR10, and DVS Gesture. Some prior works report results only in figures (denoted by *). [†] denotes our implementation of TQTTFS [35]. Refer to the main text or Supplementary Material for more details about symbolic representations of the network structure. SCNN¹ [35] is C16K5-P2-C32K5-P2-FC128-FC10. SCNN² [83] is C6K5-P2-C16K5-P2-FC400-FC400-10. SCNN³ [83] is C32K3-P2-C64K3-P2-C128K3-P2-FC10. SCNN⁴ [84] is C40K5-P2-FC1000-FC10. SCNN⁵ [84] is C20K5-P2-C40K5-P2-FC1000-FC10. SCNN⁶ [18] is $\{\{C256K3\} * 3 - P2\} * 2 - FC2048 - FC10$. SCNN⁷ [18] is $\{C128K3 - P2\} * 5 - FC512 - FC11$.

Method	MNIST		Fashion-MNIST		CIFAR10		DVS Gesture	
	Model	Acc.	Model	Acc.	Model	Acc.	Model	Acc.
Conversion								
TTFS clamped [51]	LeNet-5	98.53%	-	-	-	-	-	-
LC-TTFS [85]	-	-	-	-	VGG-16	92.72%	-	-
T2FSNN [86]	-	-	-	-	VGG-16	91.43%	-	-
Directly training								
Mostafa [87]	FC800-FC10	97.5%	-	-	-	-	-	-
Comsa et al. [88]	FC340-FC10	97.9%	-	-	-	-	-	-
Göltz et al. [89]	FC350-FC10	97.2%	-	-	-	-	-	-
S4NN [53]	FC600-FC10	97.4%	FC1000-FC10	88.0%	-	-	-	-
BS4NN [63]	FC600-FC10	97.0%	FC1000-FC10	87.3%	-	-	-	-
Zhang et al. [82]	FC400-FC10	98.1%	SCNN ¹	90.1%	-	-	-	-
Sakemi et al. [83]	SCNN ²	99.25%*	SCNN ²	89.5%*	SCNN ³	80.0%*	-	-
STiDi-BP [84]	SCNN ⁴	99.2%	SCNN ⁵	92.8%	-	-	-	-
TQTTFS [35]	FC400-FC10	98.6%	FC400-FC400-FC10 SCNN ¹	88.1% 90.2%	SCNN ⁶	67.47 % [†]	SCNN ⁷	88.89% [†]
ETTFS (ours)	FC400-FC10	98.67%	FC400-FC400-FC10	90.21%	SCNN ⁶	90.56%	SCNN ⁷	95.83%
	SCNN ¹	99.48%	SCNN ⁵	92.90%				

4. Experiments

In this section, we evaluate accuracy, latency, and ablation studies for proposed methods using the SpikingJelly framework [32], with training details in Supplementary Material.

4.1. Comparison with the State-of-the-Art

We evaluate ETTFS on static (MNIST, Fashion-MNIST, CIFAR10) and neuromorphic (DVS Gesture [90]) datasets. DVS Gesture’s temporal complexity makes it particularly challenging for TTFS SNNs. To the best of our knowledge, there is no accuracy report of TTFS SNNs on it. We reuse network structures from prior work for fairness. Notation: FCn (fully-connected layer, n output features), CmKn (convolution, m output channels, n kernel size), Pn (pooling, stride n), $\{\dots\} * n$ (repetitive structures), e.g., $\{FC10\} * 2$ represents FC10-FC10. Input dimensions are omitted.

4.1.1. Accuracy

Table 1 compares our method with conversion and directly training approaches. Our framework outperforms all direct methods across datasets, notably achieving 90.56% on CIFAR10 (10.56% higher than Sakemi et al. [83]) and 95.83% on DVS Gesture (6.94% higher than TQTTFS [35]; note that their results are reproduced by us). Our accuracy is lower than conversion methods that use the large VGG-16 network structure in CIFAR10 datasets. Note that VGG-16 has 138.36M parameters, while our spiking convolu-

Table 2. Comparison of time-steps on MNIST, Fashion-MNIST, CIFAR10, and DVS Gesture datasets. Each element denotes: inference time-steps (training time-step). Some prior works report results only in figures (denoted by *). [†] denotes our implementation of TQTTFS [35].

Method	MNIST	Fashion-MNIST	CIFAR10	DVS Gesture
T2FSNN [86]	20* (40)	-	400* (680)	-
Mostafa [87]	3.5* (5*)	-	-	-
Comsa et al. [88]	20* (50*)	-	-	-
S4NN [53]	89.7 (256)	-	-	-
BS4NN [63]	112.2* (256)	100.20* (256)	-	-
STiDi-BP [84]	71.1 (100)	61.3 (100)	-	-
TQ-TTFS [35]	2.93 [†] (8)	4.21 [†] (8)	4.62 [†] (8)	4.08 [†] (8)
ETTFS (ours)	1.01 (8)	2.03 (8)	2.93 (8)	1.20 (8)

tional neural network (SCNN) contains only 70.11M parameters. Meanwhile, these conversion methods are based on layer-by-layer propagation, causing high inference latency on neuromorphic chips. Direct training methods (like ours) run SNNs in step-by-step propagation mode, aligning with neuromorphic chips’ asynchronous event processing.

4.1.2. Latency

One of the most interesting advantages of TTFS SNNs over traditional SNNs is that the inference is finished as long as any neuron in the output layer fires. Thus, the number

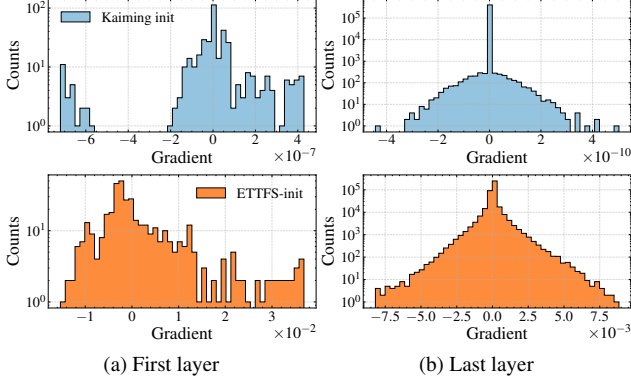


Figure 5. Comparison of gradients of weights from TTFS SNNs initialized by the Kaiming initialization (first row) and the proposed ETTFs-init method (second row). We show the histogram of $\frac{\partial \mathcal{L}}{\partial W^l}$ from (a) the first layer ($l = 0$), and (b) the last layer ($l = 4$). The Kaiming initialization results in extremely small gradients in the scale less than 10^{-7} . While our ETTFs-init method leads to appropriate gradients in the scale larger than 10^{-3} .

of time-steps of TTFS SNNs during inference is not equal to, but smaller than that of training in most cases. Table 2 compares the number of time-steps, averaged over the test set. T2FSNN [86], as a conversion method, requires substantially more simulation time-steps than other methods. This gap even widens in physical deployments because it can only run in layer-by-layer propagation. TQ-TTFS [35] and our method achieve the lowest training time-steps across all datasets, demonstrating TTFS SNNs’ efficiency via step-by-step propagation. Our approach further reduces inference time-steps through temporal weighting decoding, enabling theoretically lower energy consumption and faster inference than prior works.

4.2. Ablation Study

Our methods achieve high accuracy and low latency compared to prior work. We conduct ablation studies to examine each component’s impact on TTFS SNNs.

4.2.1. ETTFs-init on Backward Propagation

The default Kaiming initialization method causes a small variance of post-synaptic currents, $\mathbb{D}(X^l) = \frac{1}{3T}$, which does not decouple from T . Our ETTFs-init method rectifies the variance to $\mathbb{D}(X^l) = 1$. Figure 1a and 1b compare the distribution of X^l using two initialization methods on Fashion-MNIST. We further analyze backward propagation gradients through weight gradients $\frac{\partial \mathcal{L}}{\partial W^l}$ in a five-layer TTFS SNN (Figure 5). With Kaiming initialization, gradients scale from 10^{-7} to 10^{-10} across layers, correlating with diminishing post-synaptic currents in Figure 1a. In contrast, ETTFs-init maintains stable gradient scales, mitigating vanishing gradients.

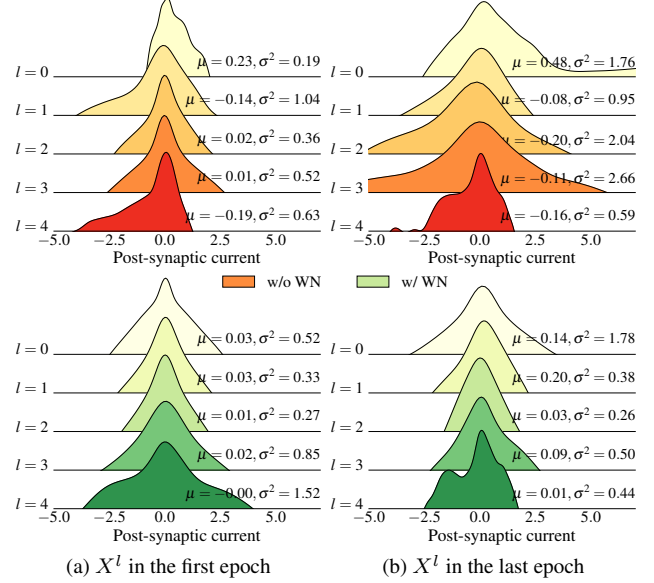


Figure 6. Comparison of the distribution of X^l during training with the ETTFs-init method only (first row) and additional weight normalization (WN) method (second row). Without normalization, the distribution of X^l shifts significantly as the epoch increases. With normalization, the distribution of X^l remains stable and shifts only minimally.

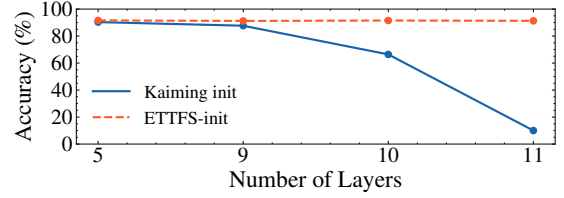


Figure 7. Evaluation of the stability of ETTFs-init on Fashion-MNIST. Layer number 5 denotes the original SCNN model, and we increase the layer number to 11 by adding linear layers.

4.2.2. Verification on Deep TTFS SNNs

Deep networks offer greater expressive power and parameter efficiency [91], yet deeper architectures face training instability, partially addressed by initialization. We compare the accuracy of TTFS SNNs with depths from 5 to 11 initialized with the Kaiming method and the ETTFs-init method. The 5-layer baseline SCNN is expanded to 11 layers through the insertion of 800-feature linear layers. Figure 7 shows that models using Kaiming initialization suffer significant accuracy degradation with depth, failing to converge at 11 layers. In contrast, ETTFs-init maintains convergence and superior accuracy, demonstrating enhanced training stability for deeper architectures.

4.2.3. Shifting and Normalization

While ETTFs-init provides stable initialization, post-synaptic currents still shift during training. Figure 6 shows

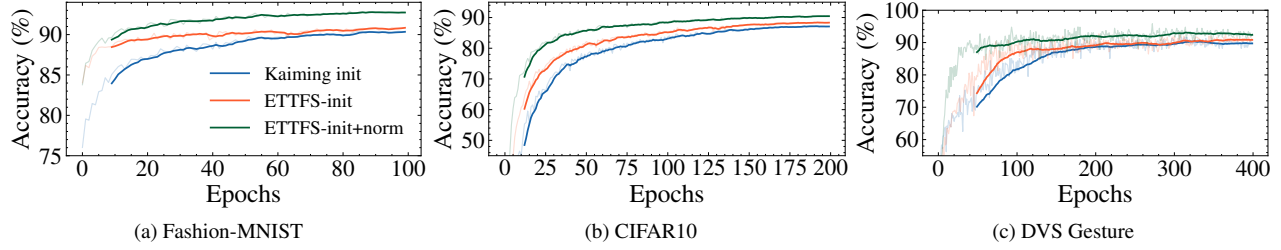


Figure 8. Comparison of the epoch-accuracy curves of Kaiming and ETTFs initialization methods on three datasets. The curves in dark colors represent the moving average of test accuracy, while the original data are plotted in light colors.

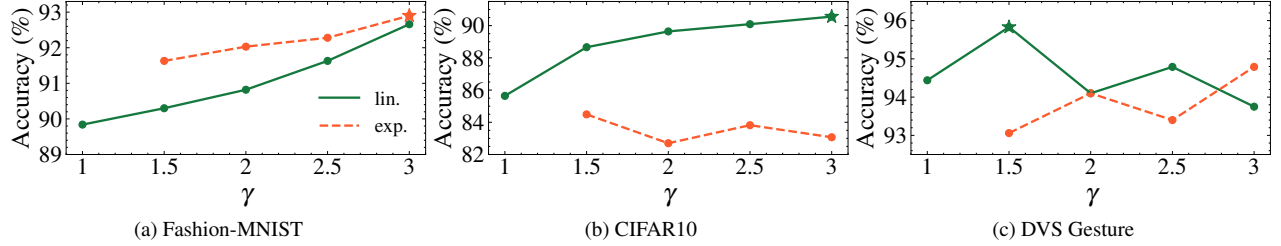


Figure 9. Comparisons of weight decay methods with different parameter values for the temporal weighting decoding method on three datasets. The highest accuracy on each dataset is marked by \star .

significant distribution shifts, particularly in deeper layers (e.g., X^2 , X^3) when weight normalization is not used on Fashion-MNIST. When equipped with weight normalization, these shifts are prevented and stable the distribution of X^l are maintained throughout training.

4.2.4. Training Curves

Furthermore, we compare the epoch-accuracy curves during training of Kaiming initialization and ETTFs-init methods across three datasets as shown in Figure 8. Consistent across benchmarks, ETTFs-init accelerates convergence and achieves higher accuracy than Kaiming initialization. With normalization enabled, performance improves further, confirming the combined method’s effectiveness.

4.2.5. Weight Decay Strategies for Temporal Decoding

Both exponential (Eq. (21)) and linear (Eq. (22)) decay prioritize early firing through temporal weighting. Larger γ values emphasize earlier spikes but introduce a risk of vanishing gradients due to suppressed later weights. We assess decay methods and γ values across three datasets. For Fashion-MNIST (Figure 9a), accuracy generally improves with increasing γ in both decay methods, peaking at $\gamma = 3$ using exponential decay. On CIFAR10 (Figure 9b), the accuracy of linear decay slightly increases and reaches its highest value at $\gamma = 3$, while exponential decay remains stable. DVS Gesture (Figure 9c) exhibits stable accuracy for both methods. This dataset-specific behavior suggests empirical optimization without generalizable guidelines.

Table 3. Evaluating framework components on the Fashion-MNIST dataset. TWD denotes temporal weighting decoding. The baseline uses max-pooling and TQ-TTFS decoding method [35].

ETTFs-init	Avg-pooling	Norm	Norm with affine	TWD	Accuracy
					89.61%
				✓	89.72%
✓				✓	90.47%
	✓			✓	90.41%
✓	✓			✓	90.88%
✓	✓	✓		✓	91.61%
✓	✓		✓	✓	92.90%

4.2.6. Accuracy Contributions

We evaluate each component of our framework (initialization, normalization, pooling choices, affine transforms, etc.) on Fashion-MNIST (Table 5). The baseline TTFS SNN with max-pooling and TQ-TTFS decoding [35] achieves 89.61% accuracy. Temporal weighting decoding improves accuracy to 89.72%. Initialization boosts to 90.47%, while average-pooling replacement reaches 90.41%. Combining initialization and average-pooling yields 90.88%, further enhanced by weight normalization (91.61%) and affine transforms (92.90%), demonstrating component effectiveness and synergistic benefits.

5. Conclusion

In this article, we propose an efficient TTFS training framework that includes weight initialization, normalization, temporal weighting decoding, and re-evaluation of pooling layers. ETTFS-init stabilizes the distribution of synaptic current in forward and mitigates vanishing gradients in backward. Weight normalization alleviates parameter shifting, enhances training stability, and improves accuracy. Temporal weighting decoding enables differentiable output decoding, promotes early spike timing, and reduces inference latency. Our analysis of pooling layers identifies max-pooling as unsuitable for TTFS SNNs, favoring average-pooling to preserve the one-spike characteristic. This framework enables training high-performance TTFS SNNs from scratch and achieves SOTA accuracy among existing TTFS SNNs. Future work will extend evaluation to larger datasets.

References

- [1] W. Maass, “Networks of spiking neurons: the third generation of neural network models,” *Neural networks*, vol. 10, no. 9, pp. 1659–1671, 1997. ¹
- [2] P. A. Merolla, J. V. Arthur, R. Alvarez-Icaza, A. S. Cassidy, J. Sawada, F. Akopyan, B. L. Jackson, N. Imam, C. Guo, Y. Nakamura *et al.*, “A million spiking-neuron integrated circuit with a scalable communication network and interface,” *Science*, vol. 345, no. 6197, pp. 668–673, 2014. ¹
- [3] M. Davies, A. Wild, G. Orchard, Y. Sandamirskaya, G. A. F. Guerra, P. Joshi, P. Plank, and S. R. Risbud, “Advancing neuromorphic computing with Loihi: A survey of results and outlook,” *Proceedings of the IEEE*, vol. 109, no. 5, pp. 911–934, 2021. ¹
- [4] J. Pei, L. Deng, S. Song, M. Zhao, Y. Zhang, S. Wu, G. Wang, Z. Zou, Z. Wu, W. He *et al.*, “Towards artificial general intelligence with hybrid Tianji chip architecture,” *Nature*, vol. 572, no. 7767, pp. 106–111, 2019. ¹
- [5] C. Eliasmith, T. C. Stewart, X. Choo, T. Bekolay, T. Dewolf, Y. Tang, and D. Rasmussen, “A large-scale model of the functioning brain,” *Science*, vol. 338, no. 6111, pp. 1202–1205, 2012. ¹
- [6] M. Stimberg, R. Brette, and D. F. Goodman, “Brian 2, an intuitive and efficient neural simulator,” *eLife*, vol. 8, p. e47314, 2019. ¹
- [7] D. O. Hebb, *The Organization of Behavior: a Neuropsychological Theory*, 2005. ¹
- [8] G.-q. Bi and M.-m. Poo, “Synaptic modifications in cultured hippocampal neurons: Dependence on spike timing, synaptic strength, and postsynaptic cell type,” *Journal of Neuroscience*, vol. 18, no. 24, pp. 10 464–10 472, 1998. ¹
- [9] T. Masquelier and S. J. Thorpe, “Unsupervised learning of visual features through spike timing dependent plasticity,” *PLOS Computational Biology*, vol. 3, no. 2, p. e31, 2007. ¹
- [10] P. U. Diehl and M. Cook, “Unsupervised learning of digit recognition using spike-timing-dependent plasticity,” *Frontiers in Computational Neuroscience*, vol. 9, p. 99, 2015.
- [11] S. R. Kheradpisheh, M. Ganjtabesh, S. J. Thorpe, and T. Masquelier, “StdP-based spiking deep convolutional neural networks for object recognition,” *Neural Networks*, vol. 99, pp. 56–67, 2018. ¹
- [12] Y. Cao, Y. Chen, and D. Khosla, “Spiking deep convolutional neural networks for energy-efficient object recognition,” *International Journal of Computer Vision*, vol. 113, no. 1, pp. 54–66, 2015. ¹
- [13] A. Tavanaei, M. Ghodrati, S. R. Kheradpisheh, T. Masquelier, and A. Maida, “Deep learning in spiking neural networks,” *Neural Networks*, vol. 111, pp. 47–63, 2019.
- [14] E. O. Neftci, H. Mostafa, and F. Zenke, “Surrogate gradient learning in spiking neural networks: Bringing the power of gradient-based optimization to spiking neural networks,” *IEEE Signal Processing Magazine*, vol. 36, no. 6, pp. 51–63, 2019.
- [15] D. V. Christensen, R. Dittmann, B. Linares-Barranco, A. Sebastian, M. L. Gallo, A. Redaelli, S. Slesazeck, T. Mikolajick, S. Spiga, S. Menzel, I. Valov, G. Milano, C. Ricciardi, S.-J. Liang, F. Miao, M. Lanza, T. J. Quill, S. T. Keene, A. Salleo, J. Grollier, D. Marković, A. Mizrahi, P. Yao, J. J. Yang, G. Indiveri, J. P. Strachan, S. Datta, E. Vianello, A. Valentian, J. Feldmann, X. Li, W. H. P. Pernice, H. Bhaskaran, S. Furber, E. Neftci, F. Scherr, W. Maass, S. Ramaswamy, J. Tapson, P. Panda, Y. Kim, G. Tanaka, S. Thorpe, C. Bartolozzi, T. A. Cleland, C. Posch, S. Liu, G. Panuccio, M. Mahmud, A. N. Mazumder, M. Hosseini, T. Mohsenin, E. Donati, S. Tolu, R. Galeazzi, M. E. Christensen, S. Holm, D. Ielmini, and N. Pryds, “2022 roadmap on neuromorphic computing and engineering,” *Neuromorphic Computing and Engineering*, vol. 2, no. 2, p. 022501, may 2022. [Online]. Available: <https://dx.doi.org/10.1088/2634-4386/ac4a83>
- [16] Y. Guo, X. Huang, and Z. Ma, “Direct learning-based deep spiking neural networks: a review,” *Frontiers in Neuroscience*, vol. 17, p. 1209795, 2023.
- [17] G. Li, L. Deng, H. Tang, G. Pan, Y. Tian, K. Roy, and W. Maass, “Brain-inspired computing: A systematic survey and future trends,” *Proceedings of the IEEE*, vol. 112, no. 6, pp. 544–584, 2024. ¹
- [18] W. Fang, Z. Yu, Y. Chen, T. Masquelier, T. Huang, and Y. Tian, “Incorporating learnable membrane time constant to enhance learning of spiking neural networks,” in *Proceedings of the IEEE/CVF International Conference on Computer Vision*, 2021, pp. 2661–2671. ^{1, 3, 5, 6, 16}
- [19] X. Yao, F. Li, Z. Mo, and J. Cheng, “Glif: A unified gated leaky integrate-and-fire neuron for spiking neural networks,” *Advances in Neural Information Processing Systems*, vol. 35, pp. 32 160–32 171, 2022.
- [20] L. Feng, Q. Liu, H. Tang, D. Ma, and G. Pan, “Multi-level firing with spiking ds-resnet: Enabling better and deeper directly-trained spiking neural networks,” in *Proceedings of the Thirty-First International Joint Conference on Artificial Intelligence, IJCAI-22*, L. D. Raedt, Ed. International Joint Conferences on Artificial Intelligence Organization, 7 2022, pp. 2471–2477, main Track. [Online]. Available: <https://doi.org/10.24963/ijcai.2022/343>

- [21] W. Fang, Z. Yu, Z. Zhou, D. Chen, Y. Chen, Z. Ma, T. Masquelier, and Y. Tian, "Parallel spiking neurons with high efficiency and ability to learn long-term dependencies," *Advances in Neural Information Processing Systems*, vol. 36, 2023. 1, 3
- [22] A. Sengupta, Y. Ye, R. Wang, C. Liu, and K. Roy, "Going deeper in spiking neural networks: Vgg and residual architectures," *Frontiers in neuroscience*, vol. 13, p. 95, 2019. 1
- [23] Y. Hu, H. Tang, and G. Pan, "Spiking deep residual networks," *IEEE Transactions on Neural Networks and Learning Systems*, vol. 34, no. 8, pp. 5200–5205, 2023.
- [24] W. Fang, Z. Yu, Y. Chen, T. Huang, T. Masquelier, and Y. Tian, "Deep residual learning in spiking neural networks," *Advances in Neural Information Processing Systems*, vol. 34, 2021. 3
- [25] Y. Hu, L. Deng, Y. Wu, M. Yao, and G. Li, "Advancing spiking neural networks toward deep residual learning," *IEEE Transactions on Neural Networks and Learning Systems*, pp. 1–15, 2024.
- [26] Z. Zhou, Y. Zhu, C. He, Y. Wang, S. Yan, Y. Tian, and L. Yuan, "Spikformer: When spiking neural network meets transformer," *arXiv preprint arXiv:2209.15425*, 2022.
- [27] M. Yao, J. Hu, Z. Zhou, L. Yuan, Y. Tian, B. Xu, and G. Li, "Spike-driven transformer," *Advances in neural information processing systems*, vol. 36, 2024. 3
- [28] M. Yao, J. Hu, T. Hu, Y. Xu, Z. Zhou, Y. Tian, B. XU, and G. Li, "Spike-driven transformer v2: Meta spiking neural network architecture inspiring the design of next-generation neuromorphic chips," in *The Twelfth International Conference on Learning Representations*, 2024. [Online]. Available: <https://openreview.net/forum?id=1SIBN5Xyw7>
- [29] C. Zhou, H. Zhang, Z. Zhou, L. Yu, L. Huang, X. Fan, L. Yuan, Z. Ma, H. Zhou, and Y. Tian, "QKFormer: Hierarchical spiking transformer using q-k attention," in *The Thirty-eighth Annual Conference on Neural Information Processing Systems*, 2024. [Online]. Available: <https://openreview.net/forum?id=AVd7DpiooC1,3>
- [30] Y. Wu, L. Deng, G. Li, J. Zhu, Y. Xie, and L. Shi, "Direct training for spiking neural networks: Faster, larger, better," in *Proceedings of the AAAI Conference on Artificial Intelligence*, vol. 33, no. 01, 2019, pp. 1311–1318. 1
- [31] C. Duan, J. Ding, S. Chen, Z. Yu, and T. Huang, "Temporal effective batch normalization in spiking neural networks," in *Advances in Neural Information Processing Systems*, A. H. Oh, A. Agarwal, D. Belgrave, and K. Cho, Eds., 2022. [Online]. Available: <https://openreview.net/forum?id=fLIggyQiJqz1>
- [32] W. Fang, Y. Chen, J. Ding, Z. Yu, T. Masquelier, D. Chen, L. Huang, H. Zhou, G. Li, and Y. Tian, "Spikingjelly: An open-source machine learning infrastructure platform for spike-based intelligence," *Science Advances*, vol. 9, no. 40, p. eadi1480, 2023. 1, 3, 6
- [33] J. K. Eshraghian, M. Ward, E. O. Neftci, X. Wang, G. Lenz, G. Dwivedi, M. Bennis, D. S. Jeong, and W. D. Lu, "Training spiking neural networks using lessons from deep learning," *Proceedings of the IEEE*, vol. 111, no. 9, pp. 1016–1054, 2023.
- [34] Y. Zeng, D. Zhao, F. Zhao, G. Shen, Y. Dong, E. Lu, Q. Zhang, Y. Sun, Q. Liang, Y. Zhao, Z. Zhao, H. Fang, Y. Wang, Y. Li, X. Liu, C. Du, Q. Kong, Z. Ruan, and W. Bi, "BrainCog: A spiking neural network based, brain-inspired cognitive intelligence engine for brain-inspired ai and brain simulation," *Patterns*, vol. 4, no. 8, p. 100789, 2023. [Online]. Available: <https://www.sciencedirect.com/science/article/pii/S26663899230014471>
- [35] Y. Yang, Z. Xuan, and Y. Kang, "Tq-ttfs: High-accuracy and energy-efficient spiking neural networks using temporal quantization time-to-first-spike neuron," in *2024 29th Asia and South Pacific Design Automation Conference (ASP-DAC)*. IEEE, 2024, pp. 836–841. 1, 2, 3, 5, 6, 7, 8, 16
- [36] E. D. Adrian, "The impulses produced by sensory nerve endings: Part i," *The Journal of physiology*, vol. 61, no. 1, p. 49, 1926. 2
- [37] R. Lestienne, "Spike timing, synchronization and information processing on the sensory side of the central nervous system," *Progress in neurobiology*, vol. 65, no. 6, pp. 545–591, 2001. 2
- [38] S. Thorpe, D. Fize, and C. Marlot, "Speed of processing in the human visual system," *nature*, vol. 381, no. 6582, pp. 520–522, 1996. 2
- [39] J. O'Keefe and M. L. Recce, "Phase relationship between hippocampal place units and the eeg theta rhythm," *Hippocampus*, vol. 3, no. 3, pp. 317–330, 1993. 2
- [40] S. Thorpe and J. Gautrais, "Rank order coding," in *Computational Neuroscience: Trends in Research, 1998*. Springer, 1998, pp. 113–118. 2
- [41] G. Portelli, J. M. Barrett, G. Hilgen, T. Masquelier, A. Maccione, S. Di Marco, L. Berdondini, P. Kornprobst, and E. Sernagor, "Rank order coding: a retinal information decoding strategy revealed by large-scale multielectrode array retinal recordings," *eNeuro*, vol. 3, no. 3, 2016. [Online]. Available: <https://www.eneuro.org/content/3/3/ENEURO.0134-15.20162>
- [42] B. Rueckauer, I.-A. Lungu, Y. Hu, M. Pfeiffer, and S.-C. Liu, "Conversion of continuous-valued deep networks to efficient event-driven networks for image classification," *Frontiers in neuroscience*, vol. 11, p. 682, 2017. 2
- [43] B. Han, G. Srinivasan, and K. Roy, "Rmp-snn: Residual membrane potential neuron for enabling deeper high-accuracy and low-latency spiking neural network," in *Proceedings of the IEEE/CVF Conference on Computer Vision and Pattern Recognition (CVPR)*, 2020, pp. 13 558–13 567.
- [44] Y. Li, S. Deng, X. Dong, R. Gong, and S. Gu, "A free lunch from ann: Towards efficient, accurate spiking neural networks calibration," in *International Conference on Machine Learning*. PMLR, 2021, pp. 6316–6325.
- [45] T. Bu, W. Fang, J. Ding, P. Dai, Z. Yu, and T. Huang, "Optimal ann-snn conversion for high-accuracy and ultra-low-latency spiking neural networks," in *International Conference on Learning Representations*, 2021.
- [46] Y. Hu, Q. Zheng, X. Jiang, and G. Pan, "Fast-snn: Fast spiking neural network by converting quantized ann," *IEEE*

- Transactions on Pattern Analysis and Machine Intelligence*, vol. 45, no. 12, pp. 14 546–14 562, 2023. 2
- [47] R. Van Rullen and S. J. Thorpe, “Rate coding versus temporal order coding: what the retinal ganglion cells tell the visual cortex,” *Neural computation*, vol. 13, no. 6, pp. 1255–1283, 2001. 2
- [48] S. Sharmin, N. Rathi, P. Panda, and K. Roy, “Inherent adversarial robustness of deep spiking neural networks: Effects of discrete input encoding and non-linear activations,” in *Computer Vision—ECCV 2020: 16th European Conference, Glasgow, UK, August 23–28, 2020, Proceedings, Part XXIX* 16. Springer, 2020, pp. 399–414.
- [49] Y. Kim, H. Park, A. Moitra, A. Bhattacharjee, Y. Venkatesha, and P. Panda, “Rate coding or direct coding: Which one is better for accurate, robust, and energy-efficient spiking neural networks?” in *ICASSP 2022-2022 IEEE International Conference on Acoustics, Speech and Signal Processing (ICASSP)*. IEEE, 2022, pp. 71–75.
- [50] K. Wu, M. Yao, Y. Chou, X. Qiu, R. Yang, B. Xu, and G. Li, “Rsc-snn: Exploring the trade-off between adversarial robustness and accuracy in spiking neural networks via randomized smoothing coding,” in *Proceedings of the 32nd ACM International Conference on Multimedia*, 2024, pp. 2748–2756. 2
- [51] B. Rueckauer and S.-C. Liu, “Conversion of analog to spiking neural networks using sparse temporal coding,” in *2018 IEEE international symposium on circuits and systems (ISCAS)*. IEEE, 2018, pp. 1–5. 2, 6
- [52] H. Mostafa, B. U. Pedroni, S. Sheik, and G. Cauwenberghs, “Fast classification using sparsely active spiking networks,” in *2017 IEEE International Symposium on Circuits and Systems (ISCAS)*, 2017, pp. 1–4. 2
- [53] S. R. Kheradpisheh and T. Masquelier, “Temporal backpropagation for spiking neural networks with one spike per neuron,” *International journal of neural systems*, vol. 30, no. 06, p. 2050027, 2020. 2, 3, 6
- [54] S. Park, S. Kim, H. Choe, and S. Yoon, “Fast and efficient information transmission with burst spikes in deep spiking neural networks,” in *Proceedings of Annual Design Automation Conference (DAC)*, 2019, pp. 1–6. 2
- [55] Y. Li and Y. Zeng, “Efficient and accurate conversion of spiking neural network with burst spikes,” 2022. 2
- [56] J. Kim, H. Kim, S. Huh, J. Lee, and K. Choi, “Deep neural networks with weighted spikes,” *Neurocomputing*, vol. 311, pp. 373–386, 2018. 2
- [57] Y. Chen, H. Qu, M. Zhang, and Y. Wang, “Deep spiking neural network with neural oscillation and spike-phase information,” *Proceedings of the AAAI Conference on Artificial Intelligence*, vol. 35, no. 8, pp. 7073–7080, May 2021. [Online]. Available: <https://ojs.aaai.org/index.php/AAAI/article/view/16870> 2
- [58] S. Thorpe, A. Delorme, and R. Van Rullen, “Spike-based strategies for rapid processing,” *Neural Networks*, vol. 14, no. 6-7, pp. 715–725, 2001. 2
- [59] R. S. Johansson and I. Birznieks, “First spikes in ensembles of human tactile afferents code complex spatial fingertip events,” *Nature neuroscience*, vol. 7, no. 2, pp. 170–177, 2004.
- [60] T. Gollisch and M. Meister, “Rapid neural coding in the retina with relative spike latencies,” *science*, vol. 319, no. 5866, pp. 1108–1111, 2008. 2
- [61] L. Zhang, S. Zhou, T. Zhi, Z. Du, and Y. Chen, “Tdsnn: From deep neural networks to deep spike neural networks with temporal-coding,” in *Proceedings of the AAAI conference on artificial intelligence*, vol. 33, no. 01, 2019, pp. 1319–1326. 2
- [62] A. Stanojevic, S. Woźniak, G. Bellec, G. Cherubini, A. Pantazi, and W. Gerstner, “An exact mapping from relu networks to spiking neural networks,” *Neural Networks*, vol. 168, pp. 74–88, 2023. 2
- [63] S. R. Kheradpisheh, M. Mirsadeghi, and T. Masquelier, “Bs4nn: Binarized spiking neural networks with temporal coding and learning,” *Neural Processing Letters*, vol. 54, no. 2, pp. 1255–1273, 2022. 2, 6
- [64] A. Stanojevic, S. Woźniak, G. Bellec, G. Cherubini, A. Pantazi, and W. Gerstner, “High-performance deep spiking neural networks with 0.3 spikes per neuron,” *Nature Communications*, vol. 15, no. 1, p. 6793, 2024. 2
- [65] Z. Wang, X. Gu, R. S. M. Goh, J. T. Zhou, and T. Luo, “Efficient spiking neural networks with radix encoding,” *IEEE Transactions on Neural Networks and Learning Systems*, vol. 35, no. 3, pp. 3689–3701, 2022. 2
- [66] S. Zhou, X. Li, Y. Chen, S. T. Chandrasekaran, and A. Sanyal, “Temporal-coded deep spiking neural network with easy training and robust performance,” in *Proceedings of the AAAI conference on artificial intelligence*, vol. 35, no. 12, 2021, pp. 11 143–11 151. 2
- [67] M. Yao, O. Richter, G. Zhao, N. Qiao, Y. Xing, D. Wang, T. Hu, W. Fang, T. Demirci, M. De Marchi *et al.*, “Spike-based dynamic computing with asynchronous sensing-computing neuromorphic chip,” *Nature Communications*, vol. 15, no. 1, p. 4464, 2024. 3
- [68] N. Rathi and K. Roy, “Diet-snn: A low-latency spiking neural network with direct input encoding and leakage and threshold optimization,” *IEEE Transactions on Neural Networks and Learning Systems*, 2021. 3
- [69] Y. Li, Y. Kim, H. Park, and P. Panda, “Uncovering the representation of spiking neural networks trained with surrogate gradient,” *Transactions on Machine Learning Research*, 2023. [Online]. Available: <https://openreview.net/forum?id=s9efQF3QW1> 3
- [70] X. Qiu, R.-J. Zhu, Y. Chou, Z. Wang, L.-J. Deng, and G. Li, “Gated attention coding for training high-performance and efficient spiking neural networks,” *Proceedings of the AAAI Conference on Artificial Intelligence*, vol. 38, no. 1, pp. 601–610, Mar. 2024. [Online]. Available: <https://ojs.aaai.org/index.php/AAAI/article/view/27816> 3
- [71] X. Glorot and Y. Bengio, “Understanding the difficulty of training deep feedforward neural networks,” in *Proceedings of the thirteenth international conference on artificial intelligence and statistics. JMLR Workshop and Conference Proceedings*, 2010, pp. 249–256. 3, 4
- [72] K. He, X. Zhang, S. Ren, and J. Sun, “Delving deep into rectifiers: Surpassing human-level performance on imagenet classification,” in *Proceedings of the IEEE International*

- Conference on Computer Vision*, 2015, pp. 1026–1034. 3, 4
- [73] W. He, Y. Wu, L. Deng, G. Li, H. Wang, Y. Tian, W. Ding, W. Wang, and Y. Xie, “Comparing snns and rnns on neuro-morphic vision datasets: Similarities and differences,” *Neural Networks*, vol. 132, pp. 108–120, 2020. 3
- [74] J. Ding, J. Zhang, Z. Yu, and T. Huang, “Accelerating training of deep spiking neural networks with parameter initialization,” 2022. [Online]. Available: <https://openreview.net/forum?id=T8BnDXDTcFZ> 3
- [75] J. Rossbroich, J. Gygax, and F. Zenke, “Fluctuation-driven initialization for spiking neural network training,” *Neuromorphic Computing and Engineering*, vol. 2, no. 4, p. 044016, 2022. 3
- [76] T. Salimans and D. P. Kingma, “Weight normalization: A simple reparameterization to accelerate training of deep neural networks,” *Advances in neural information processing systems*, vol. 29, 2016. 4
- [77] L. Huang, X. Liu, Y. Liu, B. Lang, and D. Tao, “Centered weight normalization in accelerating training of deep neural networks,” in *Proceedings of the IEEE International Conference on Computer Vision*, 2017, pp. 2803–2811.
- [78] S. Qiao, H. Wang, C. Liu, W. Shen, and A. Yuille, “Micro-batch training with batch-channel normalization and weight standardization,” *arXiv preprint arXiv:1903.10520*, 2019. 4
- [79] S. Ioffe and C. Szegedy, “Batch normalization: Accelerating deep network training by reducing internal covariate shift,” in *International conference on machine learning*. PMLR, 2015, pp. 448–456. 4
- [80] J. Lei Ba, J. R. Kiros, and G. E. Hinton, “Layer normalization,” *ArXiv e-prints*, pp. arXiv–1607, 2016. 4
- [81] Y. Wu, L. Deng, G. Li, J. Zhu, and L. Shi, “Spatio-temporal backpropagation for training high-performance spiking neural networks,” *Frontiers in neuroscience*, vol. 12, p. 331, 2018. 5
- [82] M. Zhang, J. Wang, J. Wu, A. Belatreche, B. Amornpaisannon, Z. Zhang, V. P. K. Miriyala, H. Qu, Y. Chua, T. E. Carlson *et al.*, “Rectified linear postsynaptic potential function for backpropagation in deep spiking neural networks,” *IEEE Transactions on Neural Networks and Learning Systems*, vol. 33, no. 5, pp. 1947–1958, 2021. 5, 6
- [83] Y. Sakemi, K. Yamamoto, T. Hosomi, and K. Aihara, “Sparse-firing regularization methods for spiking neural networks with time-to-first-spike coding,” *Scientific Reports*, vol. 13, no. 1, p. 22897, 2023. 6
- [84] M. Mirsadeghi, M. Shalchian, S. R. Kheradpisheh, and T. Masquelier, “Spike time displacement-based error back-propagation in convolutional spiking neural networks,” *Neural Computing and Applications*, vol. 35, no. 21, pp. 15 891–15 906, 2023. 6, 16
- [85] Q. Yang, M. Zhang, J. Wu, K. C. Tan, and H. Li, “Lc-ttfs: Towards lossless network conversion for spiking neural networks with ttfs coding,” *IEEE Transactions on Cognitive and Developmental Systems*, 2023. 6
- [86] S. Park, S. Kim, B. Na, and S. Yoon, “T2fsnn: deep spiking neural networks with time-to-first-spike coding,” in *Proceedings of the 57th ACM/EDAC/IEEE Design Automation Conference*, ser. DAC ’20. IEEE Press, 2020. 6, 7
- [87] H. Mostafa, “Supervised learning based on temporal coding in spiking neural networks,” *IEEE Transactions on Neural Networks and Learning Systems*, vol. 29, no. 7, pp. 3227–3235, 2017. 6
- [88] I. M. Comsa, K. Potempa, L. Versari, T. Fischbacher, A. Gesmundo, and J. Alakuijala, “Temporal coding in spiking neural networks with alpha synaptic function,” in *ICASSP 2020-2020 IEEE International Conference on Acoustics, Speech and Signal Processing (ICASSP)*. IEEE, 2020, pp. 8529–8533. 6
- [89] J. Göltz, L. Kriener, A. Baumbach, S. Billaudelle, O. Breitwieser, B. Cramer, D. Dold, A. F. Kungl, W. Senn, J. Schemmel *et al.*, “Fast and energy-efficient neuromorphic deep learning with first-spike times,” *Nature machine intelligence*, vol. 3, no. 9, pp. 823–835, 2021. 6
- [90] A. Amir, B. Taba, D. Berg, T. Melano, J. McKinstry, C. Di Nolfo, T. Nayak, A. Andreopoulos, G. Garreau, M. Mendoza, J. Kusnitz, M. Debole, S. Esser, T. Delbruck, M. Flickner, and D. Modha, “A low power, fully event-based gesture recognition system,” in *Proceedings of the IEEE/CVF Conference on Computer Vision and Pattern Recognition*, 2017, pp. 7243–7252. 6
- [91] L. Bottou, O. Chapelle, D. DeCoste, and J. Weston, *Scaling Learning Algorithms toward AI*, 2007, pp. 321–359. 7
- [92] M. Davies, N. Srinivasa, T.-H. Lin, G. Chinya, Y. Cao, S. H. Choday, G. Dimou, P. Joshi, N. Imam, S. Jain, Y. Liao, C.-K. Lin, A. Lines, R. Liu, D. Mathaikutty, S. McCoy, A. Paul, J. Tse, G. Venkataramanan, Y.-H. Weng, A. Wild, Y. Yang, and H. Wang, “Loihi: a neuromorphic manycore processor with on-chip learning,” *IEEE Micro*, vol. 38, no. 1, pp. 82–99, 2018. 14
- [93] M. Yao, O. Richter, G. Zhao, N. Qiao, Y. Xing, D. Wang, T. Hu, W. Fang, T. Demirci, M. De Marchi, L. Deng, T. Yan, C. Nielsen, S. Sheik, C. Wu, Y. Tian, B. Xu, and G. Li, “Spike-based dynamic computing with asynchronous sensing-computing neuromorphic chip,” *Nature Communications*, vol. 15, no. 1, p. 4464, May 2024. [Online]. Available: <https://doi.org/10.1038/s41467-024-47811-6> 14

A. Background

A.1. At-Most-One-Spike Neuronal Dynamics

The At-Most-One-Spike (AMOS) neuron executes three sequential stages: *charge*, *fire*, and *mask update* as shown in Figure 10 and the following equations:

$$H[t] = f(H[t-1], X[t]), \quad (25)$$

$$S[t] = (1 - F[t-1]) \cdot \Theta(H[t] - V_{th}), \quad (26)$$

$$F[t] = F[t-1] + S[t], \quad (27)$$

where $H[t]$ is the membrane potential, $X[t]$ is the input current, $S[t]$ is the output spike, and $F[t]$ is the firing mask at the time-step t . During charging (Eq. (25)), input $X[t]$ integrates via f to update membrane potential $H[t]$, which is retained post-spike without reset. The fire stage (Eq. (26)) emits $S[t] = 1$ only if $H[t] \geq V_{th}$ and the firing mask $F[t-1] = 0$, implemented via $(1 - F[t-1])\Theta(H[t] - V_{th})$. The mask update (Eq. (27)) permanently sets $F[t] = 1$ after firing, enforcing an irreversible refractory state through monotonic accumulation. f in Eq. (25) is the neuronal charge function specified for different neurons. For example, the formulation for the Integrate-and-Fire (IF) neuron is:

$$H[t] = H[t-1] + X[t]. \quad (28)$$

The formulation for the LIF neuron is:

$$H[t] = H[t-1] + \frac{1}{\tau_m} (- (H[t-1] - V_{rest}) + X[t]), \quad (29)$$

where τ_m is the membrane potential and V_{rest} the rest potential.

Compared with those of the traditional spiking neurons, the neuronal dynamics of the AMOS neuron do not include the neuronal reset equation. The AMOS neuron can rest after firing, which has the potential to be implemented by asynchronous neuromorphic chips to further promote energy efficiency. It is worth noting that this feature cannot be utilized by the Single Instruction Multiple Data (SIMD) computer architectures such as Graphics Processing Units (GPUs), which are currently the most powerful devices to train deep SNNs. The conditional statements of different neurons caused by the rest after firing will cause the warp divergence because the GPUs cannot execute different instructions at the same time. Then the GPUs have to execute each branch of instructions serially, and the computing efficiency is reduced. Correspondingly, using the firing mask rather than the if-else statement in neuronal dynamics is more practical for training the AMOS neuron in GPUs.

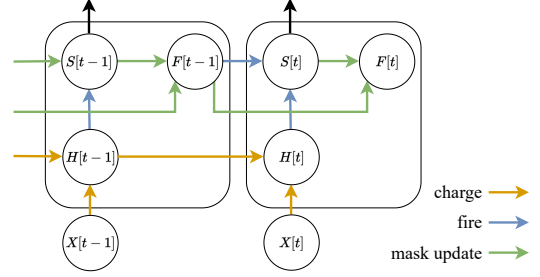


Figure 10. The neuronal dynamics of the AMOS neuron include three stages: charge, fire, and mask update. In the charge stage, the membrane potential $H[t]$ accumulates via input $X[t]$. During the fire stage, the neuron generates a spike $S[t] = 1$ if both the membrane potential $H[t]$ surpasses the threshold V_{th} and the mask $F[t-1]$ is zero; otherwise, $S[t] = 0$. The mask $F[t]$ is updated by accumulating $S[t]$ after the fire stage.

B. Derivation Details

B.1. Derivations of ETTFS-init

Without loss of generality, suppose we have an SNN stacked by L fully connected AMOS spiking neuron layers. The l -th layer can be formulated as:

$$X^l = S^{l-1}W^l, \quad (30)$$

$$S^l = \text{AMOS}(X^l). \quad (31)$$

$S^{l-1} \in \{0, 1\}^{T \times N_l}$ is the input spike from the $(l-1)$ -th layer, where T is the number of time-steps and N_l is the number of input features of the l -th layer. $W^l \in \mathbb{R}^{N_l \times M_l}$ is the weight of fully connected synapses, where M_l is the number of output features. $X^l \in \mathbb{R}^{T \times M_l}$ is the input current for the AMOS spiking neurons. $S^l \in \{0, 1\}^{T \times M_l}$ is the output spike of the l -th layer, and AMOS represents the AMOS spiking neurons. S^{l-1} keeps the one-spike characteristic: $\sum_{t=0}^{T-1} S^{l-1}[t][j] = 1$.

For $X^l[t][i]$, the i -th element of the input current at time-step t , it is calculated as:

$$X^l[t][i] = \sum_{j=0}^{n-1} S^{l-1}[t][j] \cdot W^l[j][i], \quad (32)$$

where $W^l[j][i]$ denotes the weight of the synapse from the j -th neuron in the $(l-1)$ -th layer to the i -th neuron in the

l -th layer. The variance $\mathbb{D}(X^l[t][i])$ is calculated by:

$$\begin{aligned}
\mathbb{D}(X^l[t][i]) &= \mathbb{D}\left(\sum_{j=0}^{N_l-1} S^{l-1}[t][j] \cdot W^l[j][i]\right) \\
&= N_l \cdot \mathbb{D}(S^{l-1}[t][j] \cdot W^l[j][i]) \\
&= N_l \cdot (\mathbb{E}((S^{l-1}[t][j] \cdot W^l[j][i])^2) - \mathbb{E}^2(S^{l-1}[t][j] \cdot W^l[j][i])) \\
&= N_l \cdot \mathbb{E}((S^{l-1}[t][j])^2) \cdot \mathbb{E}((W^l[j][i])^2) - 0 \\
&= N_l \sigma_{W^l}^2 \cdot \mathbb{E}((S^{l-1}[t][j])^2) \\
&= N_l \sigma_{W^l}^2 \cdot \mathbb{E}(S^{l-1}[t][j]). \tag{33}
\end{aligned}$$

Then the variance $\mathbb{D}(X^l)$ is:

$$\begin{aligned}
\mathbb{D}(X^l) &= \mathbb{E}((X^l)^2) - \mathbb{E}^2(X^l) = \mathbb{E}((X^l)^2) \\
&= \frac{1}{TM_l} \sum_{t=0}^{T-1} \sum_{i=0}^{M_l-1} \mathbb{E}((X^l[t][i])^2) \\
&= \frac{1}{TM_l} \cdot (\mathbb{D}(X^l[t][i]) + \mathbb{E}^2(X^l[t][i])) \\
&= \frac{1}{TM_l} \cdot (N_l \sigma_{W^l}^2 \cdot \mathbb{E}(S^{l-1}[t][j]) + 0) \\
&= \frac{N_l \sigma_{W^l}^2}{TM_l} \sum_{t=0}^{T-1} \sum_{i=0}^{M_l-1} \mathbb{E}(S^{l-1}[t][j]) \\
&= \frac{N_l \sigma_{W^l}^2}{TM_l} \sum_{i=0}^{M_l-1} \sum_{t=0}^{T-1} \mathbb{E}(S^{l-1}[t][j]) \\
&= \frac{N_l \sigma_{W^l}^2}{TM_l} \sum_{i=0}^{M_l-1} 1 \\
&= \frac{N_l \sigma_{W^l}^2}{T}. \tag{34}
\end{aligned}$$

B.2. Derivations of Pooling in TTFS

A more precise description is as follows. Without loss of generality, suppose there are n one-spike input sequences $S_{in} \in \{0, 1\}^{T \times n}$ in a pooling window, and the output is a spike sequence $S_{out} \in \{0, 1\}^{T \times 1}$. When using max pooling, the sum of the output spike sequence in the time-step dimension is:

$$\begin{aligned}
\sum_{t=0}^{T-1} S_{out}[t] &= \sum_{t=0}^{T-1} \max(S_{in}[t][0], S_{in}[t][1], \dots, S_{in}[t][n-1]) \\
&= \sum_{t=0}^{T-1} \min\left(\sum_{i=0}^{n-1} S_{in}[t][i], 1\right). \tag{35}
\end{aligned}$$

$\sum_{t=0}^{T-1} S_{out}[t] > 1$ occurs when there is more than one neuron in the pooling window firing at different time-steps. This violates the one-spike characteristic. Conversely, aver-

Table 4. Comparisons of accuracy of classifying the Fashion-MNIST dataset with different weight decay methods and γ in temporal weighting decoding method. We denote $w[t] = \gamma^{-t}$ as exponential decay (exp.), $w[t] = \gamma \cdot \frac{T-t}{T}$ as linear decay (lin.).

γ	Fashion-MNIST		CIFAR10		DVS Gesture	
	exp.	lin.	exp.	lin.	exp.	lin.
1	-	89.84%	-	85.64%	-	94.44%
1.5	91.63%	90.30%	84.49%	88.66%	93.06%	95.83%
2	92.03%	90.82%	82.7%	89.64%	94.10%	94.10%
2.5	92.28%	91.63%	83.82%	90.09%	93.40%	94.79%
3	92.90%	92.66%	83.07%	90.56%	94.79%	93.75%

age pooling does not suffer from this problem:

$$\sum_{t=0}^{T-1} S_{out}[t] = \sum_{t=0}^{T-1} \frac{1}{n} \sum_{i=0}^{n-1} S_{in}[t][i] = 1. \tag{36}$$

Additionally, some neuromorphic chips, such as the Loihi [92] and the Speck [93], only support the average pooling layer, which is implemented by reusing the convolutional layer to save hardware resources.

C. Temporal Weighting Decoding

We quantitatively report the results of weight decay methods and γ values on accuracy from Figure 8 in the main text. As shown in Table 4, for the Fashion-MNIST dataset, linear decay continuously improves as γ increases, achieving peak accuracy (**92.90%**) at $\gamma = 3$. CIFAR10 exhibits an inverse pattern: exponential decay shows progressive accuracy reduction with increasing γ , while linear decay improves monotonically, reaching its maximum (**90.56%**) at $\gamma = 3$. The results on DVS Gesture dataset also highlight dataset-specific dependencies: linear decay peaks earlier at $\gamma = 1.5$ (**95.83%**) and maintains stable performance with larger γ values, contrasting with the continuous improvement observed in Fashion-MNIST.

D. Comparisons of Different Proposed Methods

We evaluate the influence of ETTFs-init and weight normalization with affine transformation across three main datasets. As demonstrated in Table 5, applying ETTFs-init alone exhibits clear improvement over the baseline on Fashion-MNIST (**0.47%**), CIFAR10 (**2.10%**), and DVS Gesture (**1.04%**). Further incorporating weight normalization with affine transformation significantly boosts performance on Fashion-MNIST (**2.02%**), CIFAR10 (**2.98%**), and DVS Gesture (**3.12%**) respectively compared to using only ETTFs-init. These results demonstrate that the proposed ETTFs-init and weight normalization methods have strong generalizability and can maximize performance.

Table 5. Comparisons of performance with different proposed methods on the Fashion-MNIST, CIFAR10, and DVS Gesture datasets.

Dataset	ETTFS-init	Norm with affine	Accuracy
Fashion-MNIST			90.41%
	✓		90.88%
	✓	✓	92.90%
CIFAR10			87.32%
	✓		88.59%
	✓	✓	90.56%
DVS Gesture			91.67%
	✓		92.71%
	✓	✓	95.83%

Table 6. Experimental settings on MNIST, Fashion-MNIST, CIFAR10, and DVS Gesture datasets. LR denotes learning rate, DA denotes data augmentation.

Dataset	Fashion-MNIST & MNIST	CIFAR10	DVS Gesture
Batch size	128	64	16
Epochs	100	200	400
Optimizer	AdamW	SGD	AdamW
LR	$1e-3$	$1e-6 \rightarrow 0.1$	$1e-6 \rightarrow 0.1$
Loss function	MSE	CrossEntropy	MSE
Time step	8	8	8
DA	Mixup	Mixup, cutmix, horizontal flip, autoaugment, random erase	Random temporal delete

E. Experimental Settings

To ensure reproducibility, we provide all experimental settings in Table 6. Additionally, all source code, trained model weights, and training logs for each benchmark are included in the Supplementary Material, enabling full replication of our results.

F. Architectures

For a fair comparison, we use the same network structures from previous methods. The detailed layer descriptions and output sizes can be found in Table 7.

Table 7. Detailed architecture on MNIST, Fashion-MNIST, CIFAR10, and DVS Gesture. SCNN¹ [35] is C16K5-P2-C32K5-P2-FC128-FC10. SCNN⁵ [84] is C20K5-P2-C40K5-P2-FC1000-FC10. SCNN⁶ [18] is $\{\{C256K3\} * 3 - P2\} * 2 - FC2048 - FC10$. SCNN⁷ [18] is $\{C128K3 - P2\} * 5 - FC512 - FC11$.

#	Layer Description	output size
FC400-FC10 (MNIST)		
FC400	lin. $28 \times 28, 400$	$T \times 400$
FC10	lin. 400, 10	$T \times 10$
TWD	temporal weighting decoding	10
FC400-FC400-FC10 (Fashion-MNIST)		
FC400	lin. $28 \times 28, 400$	$T \times 400$
FC400	lin. 400, 400	$T \times 400$
FC10	lin. 400, 10	$T \times 10$
TWD	temporal weighting decoding	10
SCNN¹ (MNIST)		
C16K5	conv. $1 \times 5 \times 5 \times 16$ stride 1	$T \times 16 \times 24 \times 24$
P2	avg. 2×2	$T \times 16 \times 12 \times 12$
C32K5	conv. $16 \times 5 \times 5 \times 32$ stride 1	$T \times 32 \times 8 \times 8$
P2	avg. 2×2	$T \times 32 \times 4 \times 4$
FC800	lin. 512, 800	$T \times 800$
FC128	lin. 800, 128	$T \times 128$
FC10	lin. 800, 10	$T \times 10$
TWD	temporal weighting decoding	10
SCNN⁵ (Fashion-MNIST)		
C20K5	conv. $1 \times 5 \times 5 \times 20$ stride 1	$T \times 20 \times 24 \times 24$
P2	avg. 2×2	$T \times 20 \times 12 \times 12$
C40K5	conv. $20 \times 5 \times 5 \times 40$ stride 1	$T \times 40 \times 8 \times 8$
P2	avg. 2×2	$T \times 40 \times 4 \times 4$
FC1000	lin. 640, 1000	$T \times 1000$
FC10	lin. 1000, 10	$T \times 10$
TWD	temporal weighting decoding	10

#	Layer Description	output size
SCNN⁶ (CIFAR10)		
C256K3*3	conv. $3 \times 3 \times 3 \times 256$ stride 1 *3	$T \times 256 \times 32 \times 32$
P2	avg. 2×2	$T \times 256 \times 16 \times 16$
C256K3*3	conv. $256 \times 3 \times 3 \times 256$ stride 1 *3	$T \times 256 \times 16 \times 16$
P2	avg. 2×2	$T \times 256 \times 8 \times 8$
FC800	lin. 16384, 4096	$T \times 4096$
FC128	lin. 4096, 10	$T \times 10$
TWD	temporal weighting decoding	10
SCNN⁷ (DVS Gesture)		
C128K3	conv. $2 \times 3 \times 3 \times 128$ stride 1	$T \times 128 \times 128 \times 128$
P2	avg. 2×2	$T \times 256 \times 64 \times 64$
C128K3	conv. $2 \times 3 \times 3 \times 128$ stride 1	$T \times 128 \times 64 \times 64$
P2	avg. 2×2	$T \times 256 \times 32 \times 32$
C128K3	conv. $2 \times 3 \times 3 \times 128$ stride 1	$T \times 128 \times 32 \times 32$
P2	avg. 2×2	$T \times 256 \times 16 \times 16$
C128K3	conv. $2 \times 3 \times 3 \times 128$ stride 1	$T \times 128 \times 16 \times 16$
P2	avg. 2×2	$T \times 256 \times 8 \times 8$
C128K3	conv. $2 \times 3 \times 3 \times 128$ stride 1	$T \times 128 \times 8 \times 8$
P2	avg. 2×2	$T \times 256 \times 4 \times 4$
FC800	lin. 2048, 512	$T \times 512$
FC128	lin. 512, 11	$T \times 11$
TWD	temporal weighting decoding	11